Marine Geology 337 (2013) 195–201

Contents lists available at SciVerse ScienceDirect

Marine Geology

journal homepage: www.elsevier.com/locate/margeo

Letter

Palynology: A tool to identify abrupt events? An example from Chabahar Bay, southern Iran

Ch.S. Miller [a,*], S.A.G. Leroy [a], G. Izon [b,c], H.A.K. Lahijani [d], F. Marret [e], A.B. Cundy [f,1], P.A. Teasdale [f,1]

[a] Institute for the Environment, Brunel University, Kingston Lane, Uxbridge, London, UB8 3PH, UK
[b] Department of Earth Sciences, University of St. Andrews, North Street, St. Andrews KY16 9AL, UK
[c] School of Earth and Environment, University of Leeds, Woodhouse Lane, Leeds LS2 1JT, UK
[d] Iranian National Institute for Oceanography (INIO), No. 3, Etemadzadeh St., Fatemi Ave., 12 Tehran 1411813389, Iran
[e] School of Environmental Sciences, University of Liverpool, L69 7ZT Liverpool, UK
[f] University of Brighton, School of Environment and Technology, Brighton, BN2 4GJ, UK

ARTICLE INFO

Article history:
Received 25 October 2012
Received in revised form 19 March 2013
Accepted 24 March 2013
Available online 1 April 2013

Communicated by J.T. Wells

Keywords:
palynology
palaeoevent
Sea of Oman
flood
storm
tsunami

ABSTRACT

Tsunami, storm and flood events are destructive agents that have the potential to cause much damage and cost lives. The coastal regions around the north-western Arabian Sea are prone to these natural disasters with recent events including the storm and flood of AD 1842, the Makran tsunami of 1945, and Cyclone Gonu in 2007. Despite their severity, the paucity of reliable historical records does not allow us to answer pertinent questions concerning their frequency, intensity and impact. Palaeo-event analysis from the geological record allows us to extend, and test, the historical record. Here we have dated and examined a 92 cm long sediment core from the tectonically active, cyclone and storm prone Chabahar Bay area (southern Iran). Our appraisal directly tests conventional proxies for identifying abrupt events (*e.g.* grain-size, geochemical data), which we supplement with a novel palynological (pollen and dinocyst) approach. Both sedimentological and palynological approaches suggest a large event which was dated at <AD 1808 ± 41, whereas geochemical approaches remain inconclusive. The increase of continentally derived pollen (Pinaceae, *Salix*, *Betula* and *Typha–Sparganium*), increases in *Brigantedinium* sp. and *S. ramosus* as well as decreases in *Lingulodinium machaerophorum* suggest enhanced fluvial delivery in association with a flood. This investigation provides evidence of a major flash-flood affecting the Chabahar Bay region at <AD 1808 ± 41 which we infer is the geological expression of the storm and associated flash flood of AD 1842. Moreover, our study demonstrates the utility of palynology in identifying and understanding the causes of abrupt events to complement more widely applied techniques.

1. Introduction

Pozm and Chabahar Bays are located along the tectonically active Makran coast of the Sistan and Baluchistan province in SE Iran (25°25′0.60″N, 60°28′27.33″E; Fig. 1). The Makran coast is governed by the convergence of the Arabian and Eurasian plates leading to large shallow earthquakes resulting in tsunamis (Ambraseys and Melville, 1982; Byrne et al., 1992; Dominey-Howes et al., 2006; Shah-hosseini et al., 2011). The Sumatra–Andaman tsunami, which affected the Indian Ocean in 2004, claimed nearly 250,000 lives and served to focus scientific attention on ways to predict the frequency, intensity and possible effects of future events (Harinarayana and Hirata, 2005). The Arabian Sea is also a region of tropical cyclone development (Webster et al., 2005). Cyclone Gonu (2007), the strongest tropical cyclone on record affecting the Oman Sea, caused over 4 billion US $ in damage and 73 deaths in Oman and Iran (Fritz et al., 2010). Prior to Cyclone Gonu, three similarly destructive storms struck Oman and Iran in AD 865, AD 1842 and AD 1890, however the precise trajectories and intensities of these storms are unknown (Bailey, 1988; Knapp et al., 2010). Although rare, floods in arid regions, such as the Iranian coastline, can also cause severe damage, due to the temporal variability of rainfall and the scarcity of plant cover (Al-Qurashi, 2010).

The sedimentary expression of tsunamis, cyclones or flash-floods within shallow marine or coastal environments is typified by changes in the grain-size (GS) distribution, with the event horizon forming a distinct sedimentary unit. The GS distribution is both water depth and source dependent according to the nature of the near- and onshore sediment (Goff et al., 2010; Chagué-Goff et al., 2011, 2012). Magnetic susceptibility (MS) has also been shown to provide additional information about the depositional environment (*e.g.* Costa et al., 2012; Ramírez-Herrera et al., 2012).

* Corresponding author at: Department of Environment, Earth and Ecosystems, CEPSAR, The Open University, MK7 6AA, UK. Tel.: +44 1908 655152; fax: +44 1908 652559.
E-mail addresses: c.s.miller@open.ac.uk (C.S. Miller), Suzanne.Leroy@brunel.ac.uk (S.A.G. Leroy), G.J.Izon@leeds.ac.uk (G. Izon), lahijani@inio.ac.ir (H.A.K. Lahijani), F.Marret@liv.ac.uk (F. Marret), A.Cundy@brighton.ac.uk (A.B. Cundy), P.A.Teasdale@brighton.ac.uk (P.A. Teasdale).
[1] Tel.: +44 1273 642270.

0025-3227 © 2013 Elsevier B.V. Open access under CC BY-NC-ND license.
http://dx.doi.org/10.1016/j.margeo.2013.03.004

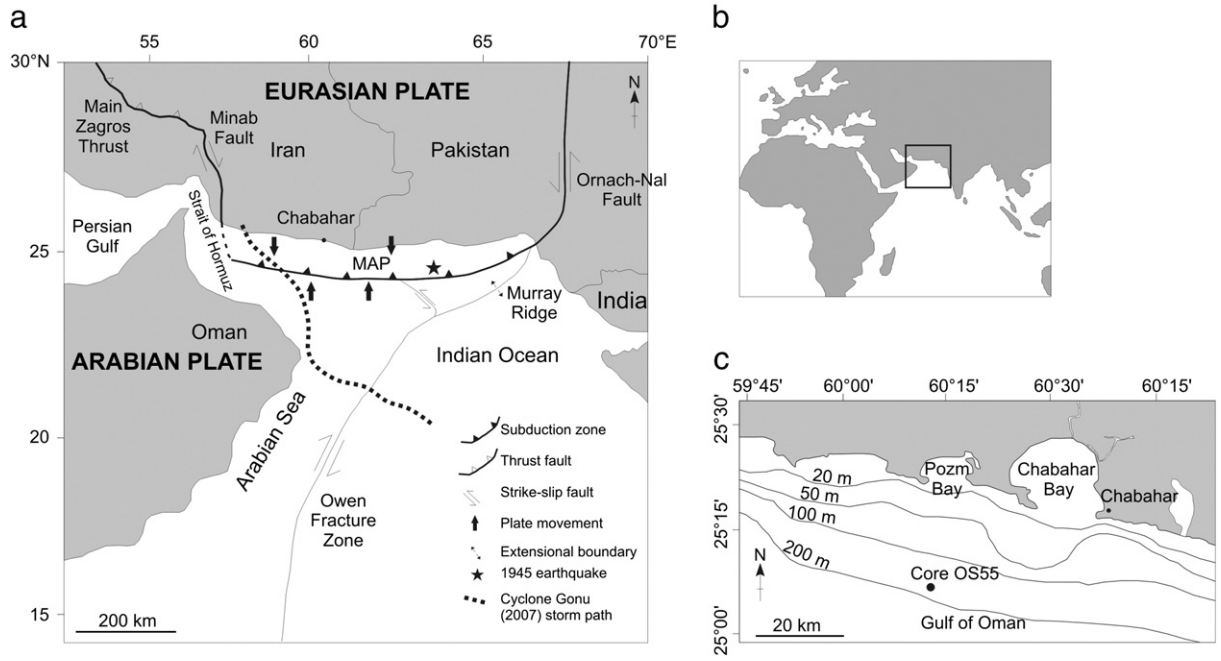

Fig. 1. Location of Oman Sea cores and the tectonic setting of the Makran in the northern Indian Ocean. a: The study region with general tectonic features (after Heidarzadeh et al., 2008). b: The western hemisphere with the region under study in inset. c: Pozm and Chabahar Bays with the location of core OS55.

Furthermore, increases in the elemental concentration of calcium, and by inference $CaCO_3$, may indicate an increase in the abundance of shell material relative to the underlying and overlying sediment (Goff et al., 2004). Additionally microfossils, such as dinoflagellate cysts (dinocysts), may display changes in assemblage governed by changes related to water parameters (Chagué-Goff et al., 2002) and pollen concentrations are often diluted in an event horizon due to increased dilution by sediment 'impoverished' in pollen relative to background sedimentation (Leroy et al., 2009; Ramírez-Herrera et al., 2012).

Currently, proxy-toolkits are available to distinguish between the sedimentary expressions of tsunamis, cyclones and flash-floods (*e.g.* Ramírez-Herrera et al., 2012); however the proposed signatures are strongly dependant on the depositional environment. Accordingly, the ability to distinguish between tsunami, storm or floods in the geological record is still a matter of considerable debate and unequivocal proxies for each deposit are yet to be fully established (*e.g.* Dawson and Shi, 2000; Goff et al., 2004; Kortekaas and Dawson, 2007; Morton et al., 2007; Horton et al., 2011; Costa et al., 2012; Goff et al., 2012). In this paper we identify an abrupt event from a core recovered from the northern Arabian Sea, southern Iran (Fig. 1). Our approach utilises widely employed techniques including: GS distributions, MS, percentage $CaCO_3$, total organic carbon (TOC), total sulphur (TS) and total nitrogen (TN) analysis, which we supplement with palynological data (pollen and dinocysts) to characterise the sediment provenance and the mechanism of deposition. These observations are then integrated with a robust ^{210}Pb based age–depth model to correlate with historical records. Accordingly, this study demonstrates the utility of a multi-proxy approach whilst illustrating the power of palynology to differentiate between different depositional mechanisms.

2. Methods

Core OS55 was retrieved in 2006 by the Iranian National Centre for Oceanography at 25° 14.27′N, 59° 48.97′E (Fig. 1c), 22 km from the coast at a water depth of 190 m. The chronology was constructed *via* ^{210}Pb and ^{137}Cs dating, using a Canberra well-type ultra-low background HPGe gamma ray spectrometer at the University of Brighton (Appleby and Oldfield, 1978; Appleby et al., 2001). Spectra were accumulated using a 16K channel integrated multichannel analyzer and analysed using the Genie™ 2000 system. Energy and efficiency calibrations were carried out using bentonite clay spiked with a mixed gamma-emitting radionuclide standard, QCYK8163, and checked against an IAEA marine sediment certified reference material (IAEA 135). Detection limits depend on radionuclide gamma energy, count time and sample mass, but were typically ~15 Bq kg^{-1} for ^{210}Pb, and 3 Bq kg^{-1} for ^{137}Cs, for a 150,000 second count time. The age′ depth model for core OS55 is derived from the simple and constant rate of supply (CRS) models of ^{210}Pb dating, and (limited) down core extrapolation.

The volume of magnetic susceptibility was measured using a Bartington MS2 magnetic susceptibly system equipped with a MS2C whole-core logging sensor, prior to GS determination using a Cilas 1064 laser particle size analyser (including the bioclastic component). GS data were reduced using Size Expert, with graphed parameters determined offline using the Folk and Ward (1957) ϕ method in GRADISTAT (Blott and Pye, 2001). Elemental analysis, including the abundance of $CaCO_3$, TOC, TS and TN was determined on ~200 mg samples using a LECO Instruments CNS 2000 elemental analyser. The precision of this technique is deemed to be better than 0.05% based on 30 replicates of a NIST traceable LECO soil standard.

Palynological sub-samples, focussing on and around any potential event beds (as indicated by the GS analysis), were prepared using sequential acid digests as detailed in Faegri and Iversen (1989). Sample preparation avoided acetolysis to preserve dinocysts (Marret, 1993). Palynomorphs were counted to >300 grains per sample and concentration was calculated using *Lycopodium* tablets (Stockmarr, 1972). Pollen grains were identified using Faegri and Iversen (1989), Reille (1995), the online African Pollen Database (http://medias.obs-mip.fr/apd/) and PalDat (www.paldat.org). Dinocysts were identified using the papers of Zonneveld (1997a, 1997b), Zonneveld and Jurkschat (1999) and Rochon et al. (1999). Pollen and dinocyst assemblage zonations were obtained using constrained incremental sums of squares (CONISS). To

determine the dominant pattern of change through the OS55 record, we examined the pollen and dinoflagellate data using the detrended correspondence analysis technique (DCA; Bennett, 2003).

3. Results

3.1. Chronology

The CRS derived age–depth model is based on eleven ^{210}Pb determinations from bulk sediment. The unsupported ^{210}Pb specific activity curve shows a peak at 17 cm and a decrease at 10 cm (Fig. 2). The results of ^{210}Pb dating for core OS55 gave an average sedimentation rate of ~2.3 mm yr^{-1}. The oldest age derived by ^{210}Pb (at 43 cm) approximates the upper surface of a coarse grained bed. This change in mean GS (Section 3.2) at 64.5–43 cm most likely indicates a sediment influx which may invalidate the assumptions of the CRS model and prevents further down-core extrapolation. Within our chronology the upper surface of the coarse horizon at 64.5–43 cm is dated at <AD 1808 (±41). ^{137}Cs activity was also measured in core OS55 to attempt to identify the onset of high-yield atmospheric nuclear weapons testing (*e.g.* Ritchie and McHenry, 1990). ^{137}Cs activities were very low (<4 Bq/kg) and were mostly at or below the limit of detection (reflecting the relatively conservative nature of ^{137}Cs in shelf waters and/or sediment compositional effects). Given the low activities observed, it was not possible to discriminate subsurface activity maxima in ^{137}Cs that could be used to further constrain the age–depth model of core OS55.

3.2. Sediment description

Grain-size determinations from core OS55 indicate the presence of series of thinly bedded sands at ~90–88, 77–75, 28.5–27.5, 26–25, 19–17, 12–10 and 9–7 cm (Fig. 3a). An abrupt increase in GS occurs at 64.5 cm followed by a series of thick sand units interbedded with coarse silts. The sand horizons at 64.5–43 cm represent a series of transient changes punctuated by a return to typical background sedimentation. The GS analysis shows four sand beds each with erosional basal contacts, interbedded with silt. Sorting, skewness and kurtosis complement the variations in GS (Fig. 3a), with increases in mean GS corresponding to a decreased degree of sorting. For example, from 49 to 43 cm an increase in the mean GS from 7 to 14 μm corresponds to a decrease in sorting from 1.54 to 1.9 ϕ. According to Folk and Ward (1957), the whole core is poorly sorted, with the exception of a sample at 77 cm, which is very poorly sorted. The majority of core OS55 is fine or near-symmetrically skewed (Fig. 3a). Two samples at 89 and 77 cm are negatively skewed whilst samples between 64.5 and 43 cm show strong positive skewness values. Kurtosis values are highly variable, arranged around a mean of 0.84 K_G. High values of kurtosis occur at 63.5, 56.5, 47.5 and 43.5 cm, all within the 64.5–43 cm sand unit (Fig. 3a).

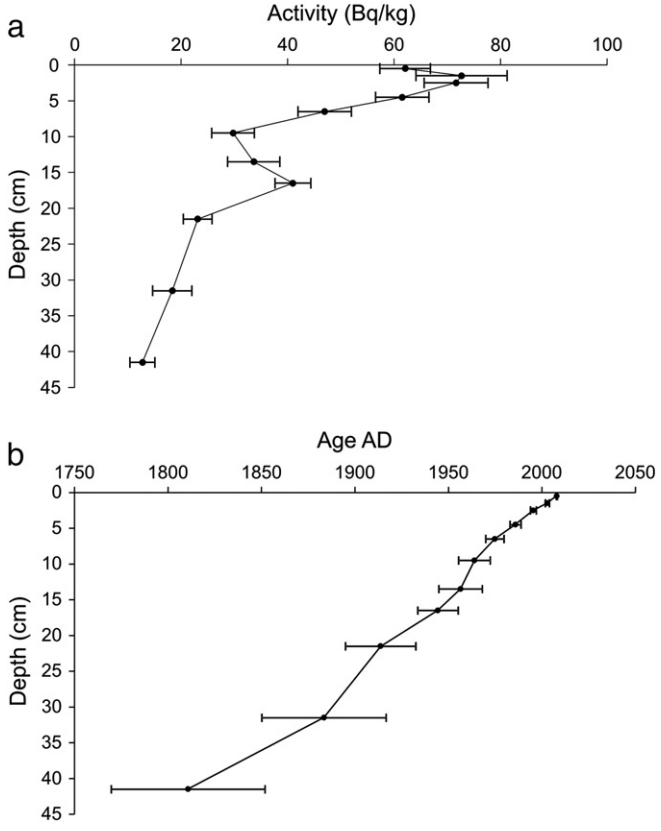

Fig. 2. a: ^{210}Pb specific activity versus depth curve. Error bars show counting error. Activity values are Bq kg^{-1} dry weight. b: The resulting age–depth model (errors calculated following Appleby et al., 2001).

3.3. Physical and geochemical properties

Magnetic susceptibility fluctuates around a mean of 4.7 SI and does not precisely correlate with changes in GS (Fig. 3a). The highest peak of MS is at 48 cm where values reach 5.5 SI. At 54 cm, MS reaches its minimum at 3.5 SI (Fig. 3a) correlating with increases in both GS and maximum wt.% $CaCO_3$. Percentage $CaCO_3$ fluctuates throughout the core, with significant peaks (>35 wt.%) at 71.5, 60.5, 52.5 cm (Fig. 3a). TOC is low and stable throughout peaking to 2.57 wt.% at 46.5 cm (Fig. 3a). TS and TN are low throughout, with mean percentages of 0.29 and 0.14 respectively, displaying little variability outside of analytical uncertainty.

3.4. Pollen analysis

The average pollen concentrations were low at *c.* 2230 grains cm^{-3} (Fig. 3b). Taxa are plotted as percentage abundances, which were calculated as a percentage of the total sum of pollen counted (excluding varia and aquatic pollen). Of the 30 samples, seventeen taxa were identified to at least family level. Generally the pollen assemblage is dominated by Chenopodiaceae, *Artemisia* and Poaceae, with sub-division of the succession into four pollen zones (Pz) by CONISS (Fig. 3b):

Pz1, 86.5 to 64.5 cm, 6 samples.
Zone Pz1 is characterised by maximum values of *Artemisia* at 74.5 cm (35%) and maximum values of *Calligonum* at 80.5 cm (10%). *Rhizophora* is present and is the only component of the mangrove species within core OS55.
Pz2, 64.5 to 48.5 cm, 12 samples.
Zone Pz2 is characterised by high values of Chenopodiaceae (35–48%), total arboreal pollen (AP; 8%), *Betula* (2%), *Salix*, undeterminable grains and *Typha–Sparganium* (3–4%). *Rhizophora* and Cyperaceae are extremely low within this zone relative to Pz1. Zone Pz2 shows fluctuations in AP, with high values of *Ephedra* and Pinaceae sp.
Pz3, 48.5 to 42.5 cm, 4 samples.
The lower part of Pz3 shows the presence of AP with the upper half showing a decrease especially in *Ephedra*, *Betula*, *Rhizophora* and *Salix*. *Typha-Sparganium* is not present in this zone and remains absent for the remainder of the core.
Pz4, 42.5 to 8.5 cm, 8 samples.
Ephedra, *Rhizophora*, *Artemisia* and *Calligonum* abundance stabilises through zone Pz4. Whereas, *Plantago rhizoxylon* and Asteraceae peak at 12.5 cm to 3.3% and 3.8% respectively. *Betula* is absent in this zone and Pinaceae percentages slowly decrease to *c.* 0% at 33.5 cm. *Rhizophora* percentages peak at 24.5 cm (1.7%).

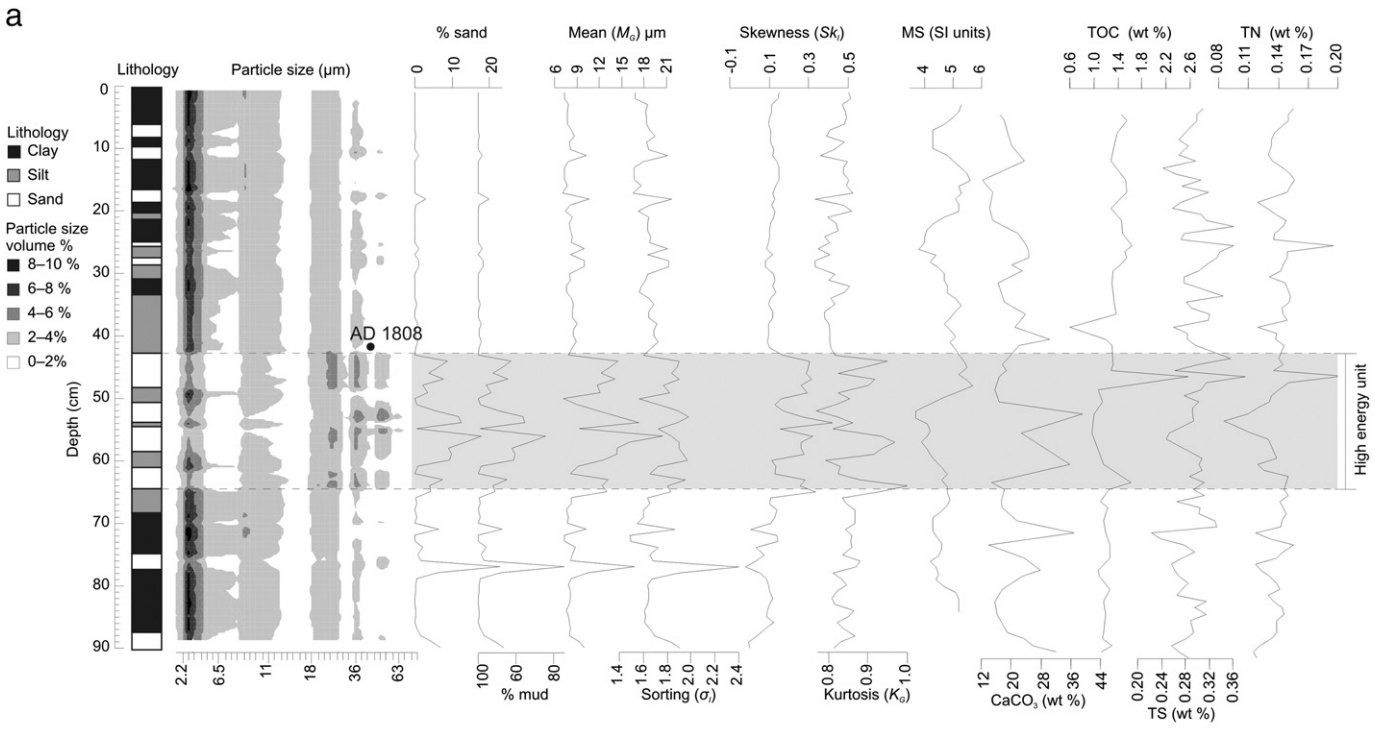
a
Lithology
Particle size (μm)
% sand
Mean (M_σ) μm
Skewness (Sk_i)
MS (SI units)
TOC (wt %)
TN (wt %)
Lithology
Clay
Silt
Sand
Particle size volume %
8–10 %
6–8 %
4–6 %
2–4%
0–2%
AD 1808
Depth (cm)
High energy unit
% mud
Sorting (σ_i)
Kurtosis (K_σ)
$CaCO_3$ (wt %)
TS (wt %)

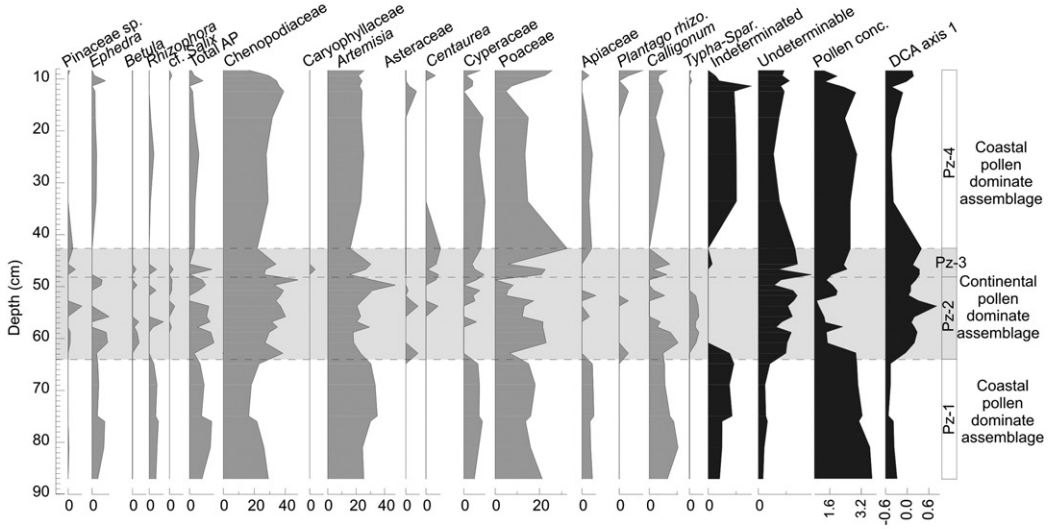
b
Pinaceae sp.
Ephedra
Betula
Rhizophora
cf. Salix
Total AP
Chenopodiaceae
Caryophyllaceae
Artemisia
Asteraceae
Centaurea
Cyperaceae
Poaceae
Apiaceae
Plantago rhizo.
Calligonum
Typha-Spar.
Indeterminated
Undeterminable
Pollen conc.
DCA axis 1
Depth (cm)
Pz-4
Coastal pollen dominate assemblage
Pz-3
Pz-2
Continental pollen dominate assemblage
Pz-1
Coastal pollen dominate assemblage

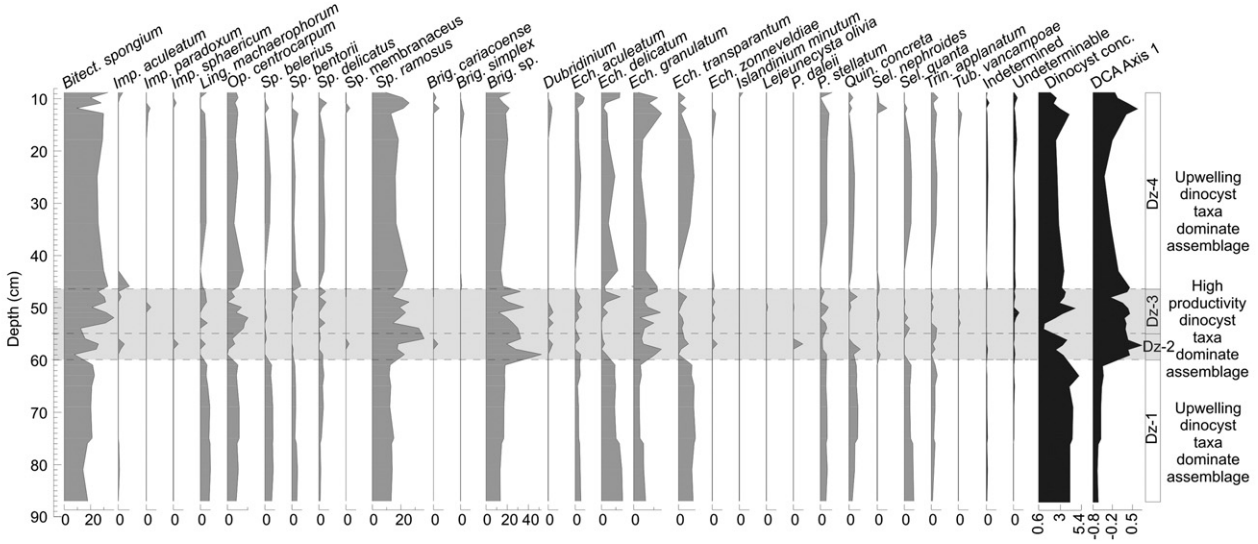
c
Bitect. spongium
Imp. aculeatum
Imp. paradoxum
Imp. sphaericum
Ling. machaerophorum
Op. centrocarpum
Sp. belerius
Sp. bentorii
Sp. delicatus
Sp. membranaceus
Sp. ramosus
Brig. cariacoense
Brig. simplex
Brig. sp.
Dubridinium
Ech. aculeatum
Ech. delicatum
Ech. granulatum
Ech. transparantum
Ech. zonneveldiae
Islandinium minutum
Lejeunecysta olivia
P. daleii
P. stellatum
Quin. concreta
Sel. nephroides
Sel. quanta
Trin. applanatum
Tub. vancampoae
Indeterminated
Undeterminable
Dinocyst conc.
DCA Axis 1
Depth (cm)
Dz-4
Upwelling dinocyst taxa dominate assemblage
Dz-3
High productivity dinocyst taxa dominate assemblage
Dz-2
Dz-1
Upwelling dinocyst taxa dominate assemblage

3.5. Dinoflagellate cyst analysis

The observed dinocyst concentrations were low, with an average of ~3320 grains cm^{-3}. In total, twenty-eight taxa were identified mostly to species level. The assemblage is dominated by *Bitectatodinium spongium*, *Spiniferites ramosus* and *Brigantedinium* sp. with subordinate amounts of *Echinidinium granulatum, E. delicatum* and *Operculodinium centrocarpum* (Fig. 3c). The dinocyst (Dz) and pollen (Pz) zonation show relatively good stratigraphic correspondance.

Dz1, 86.5 to 60 cm, 8 samples.
The assemblage in Dz1 is dominated by elevated abundances of *B. spongium* (22%), *S. ramosus* (14%), *Brigantedinium* sp. (18%) and *E. delicatum* (15%).
Dz2, 60 to 55 cm, 4 samples.
Dz2 is characterised by a sudden decrease in abundance of *B. spongium* from 21% at 60.5 cm to 7% at 58.5 cm. In addition, *O. centrocarpum, Lingulodinium machaerophorum, Spiniferites belerius, S. bentorii, S. delicatus. Echinidinium aculeatum, E. delicatum, Echinidinium transparantum, Quinquecuspis concreta and Selenopemphix quanta* also decrease. The percentages of *S. ramosus*, *Brigantedinium* sp., and *E. granulatum* increase to 28, 52 and 10% respectively. This zone marks the emergence of *Impagidinium aculeatum, I. sphaericum, Spiniferites membranaceus, Selenopemphix nephroides, Echinidinium zonneveldiae,* cysts of *Pentapharsodinium dalei and Tuberculodinium vancampoae*. The percentage of undeterminable cysts shows a minor increase relative to background levels.
Dz3, 55 to 46 cm, 8 samples.
Dz3 is characterised by an increase in *B. spongium* from 12 to 19% at 52 cm. The percentage of *S. ramosus* decreases rapidly from 32 to 15% at 53 cm. The percentage of *Brigantedinium* sp. fluctuates highly through the zone. Zone Dz3 also features *Impagidinium paradoxum*, *Lejeunecysta oliva* and *T. vancampoae*. Dz3 displays a strong decrease in dinocyst concentration at 54 cm.
Dz4, 46 cm to 8.5 cm, 10 samples.
Dz4 is characterised by the continued occurrence of the dominant species: *B. spongium*, *S. ramosus* and *Brigantedinium* sp. Several species re-emerge at the base of Dz3 including *S. belerius, E. aculeatum, E. transparantum, Protoperidinium stellatum, Q. concreta, S. quanta* and *Trinovantedinium applanatum. B. spongium* decreases at 12 cm whilst *S. ramosus, Brigantedinium* sp. *I. aculeatum* and *I. paradoxum* show only a muted increase.

3.6. Ordination

Detrended correspondence analysis (DCA) was applied to the pollen and dinocyst assemblages. Rare taxa were downweighted, as this lowers (but does not remove) the influence of low abundance species on the DCA results. Samples within Pz2, Pz3 and Dz2 and Dz3 plot with positive values on axis 1 clearly indicating the unique nature of these zones along the sequence relative to zones Pz1, Pz4, Dz1 and Dz4.

4. Discussion

4.1. Event chronology

Both the simple and CRS ^{210}Pb dating models assume a constant rate of ^{210}Pb supply (Appleby et al., 2001) and consequently it was not valid to extrapolate beyond the upper surface of the high-energy event at 43 cm (Section 3.1; Fig. 3). ^{210}Pb dates were obtained for the sediment directly above the main event unit at 64.5–43 cm and dates were calculated for the top surface of the event as *ca.* AD 1808 ± 41. From historical records large earthquakes leading to tsunamis during AD 1851 and 1864 are known to have affected the area (Quittmeyer and Jacob, 1979). Given that the age uncertainty on the identified event horizon is 41 years (Fig. 2b) the latter of these events is unlikely to have been the cause. We concede that the former event (AD 1851) is only just outside of analytical uncertainty and may, albeit unlikely, have caused the observed event horizon. In contrast, a storm producing flash floods did occur within the Arabian Sea during 1842 (Knapp et al., 2010), and although historical records of this storm are vague, it may offer an alternative depositional mechanism. In the discussion that follows, we use various criteria to discriminate between the potential mechanisms and to evaluate the effectiveness of widely employed physical and chemical techniques for identifying abrupt events.

4.2. Sedimentological characteristics

Changes in GS parameters (mean, sorting, skewness and kurtosis) indicate that the coring locality experienced repeated increases in energy levels, bringing coarser grained sediment, presumably sourced from shallower water. The closure depth of the site is approximately 50 m, therefore, these changes in GS parameters cannot be explained by reworking or changes in long or cross-shore transport (Saket and Etemad-Shahidi, 2012). The marked increases in GS also correspond to decreases in sorting, perhaps indicating that the sediments within the smaller sand beds at *c.* 90–88, 77–75, 28.5–27.5, 26–25, 19–17, 12–10 and 9–7 cm (Fig. 3a) were also a product of rapid deposition and may be smaller event horizons (Tucker, 1981). Although small sand beds exist throughout the core, attention is focussed on the coarse, poorly sorted bed between 64.5 and 43 cm, which is highlighted by both GS parameters and palynological characteristics. Typically river sands are positively skewed owing to the retention of finer component (Folk and Ward, 1957).The sediments within the event beds between 64.5 and 43 cm are positively skewed (Fig. 3a), and consequently suggest a riverine source. In contrast, two samples at 89 and 77 cm are negatively skewed, with an excess of coarse material, implying an influx of a beach derived component, following the removal of fines by repeated wave action (Folk and Ward, 1957). Skewness values suggest that the remaining samples contain a mixture of the two end-members (beach and river), consistent with the cores coastal position in close proximity to the rivers of Pozm Bay. Within core OS55 variations in kurtosis suggest differing flow characteristics of the depositing medium (Friedman, 1962; Ramanathan et al., 2009). An increase in kurtosis is uniquely observed within the high-energy event at 64.5–43 cm. Grain-size parameters do provide some information about sedimentary deposits, however no universal solution exists in order to unequivocally distinguish between different depositional environments (*e.g.* McLaren, 1981; McLaren and Bowles, 1985) with signatures not always universally applicable.

The close correspondence between MS and $CaCO_3$ abundance suggests that magnetic susceptibility in OS55 is sensitive to fluctuations in weight percentage of $CaCO_3$. In OS55 MS values generally show an inverse relationship with $CaCO_3$ abundance, possibly due to the dilution of magnetic minerals by biogenic material. TOC, TS and TN do not correlate to GS (Fig. 3a) and do not provide constraint on the emplacement mechanism of the high-energy events identified. In contrast, percentage $CaCO_3$ does show some relationship with grain-size (*e.g.* a peak in both wt.% $CaCO_3$ and % sand at 52.5 cm); implying an increase in shell matter during major high energy events.

Fig. 3. a: Sedimentological log for core OS55. Particle size distribution (μm) is shown as surface plot by volume %. Statistical grain-size analysis was performed using GRADISTAT (Blott and Pye, 2001) after Folk and Ward (1957). MS: magnetic susceptibility; TOC: total organic carbon. TS: total sulphur. TN: total nitrogen. b: Terrestrial and aquatic pollen percentage diagram for core OS55. c: Percentage dinoflagellate cyst diagram for core OS55. Pollen and dinoflagellate cyst zones are obtained by CONISS using Psimpoll. Pollen and dinocyst concentrations are in $\times 10^2$ grains cm^{-3}.

4.3. Pollen signatures

A general account of the vegetation of Iran can be found in Zohary (1973), and the study region consists of *Acacieta flavae iranica* and Nubo-Sindian classes as well as pockets of littoral saltland vegetation. Crucially, the pollen zonation closely follows the main lithological boundaries outlined in core OS55 (Fig. 3a; b). The main high-energy event (64.5–43 cm) recognised by the GS parameters is also identified by the pollen zonation, unlike the smaller events that punctuate the core. The pre-event assemblage (Pz1) contains higher percentages of coastal taxa such as *Rhizophora* and Cyperaceae, and low values of taxa associated with the continent such as *Betula*, *Salix*, Pinaceae and *Plantago rhizoxylon* (Fig. 3b). In contrast the event assemblage (Pz2 and Pz3) consists of continental taxa and decreased coastal taxa (Fig. 3b). Undeterminable grains (degraded/crumpled/corroded) are also observed to increase in the high-energy event bed, so were perhaps oxidised (or derived from pollen depleted soils) and then re-suspended by the inferred high-energy flow. Alternately, additional degradation may have occurred due to mechanical abrasion of the pollen during mass transport (Twiddle and Bunting, 2010). Pollen concentration also decreases in Pz2 and Pz3 suggestive of an increase in sedimentation rate and consequent dilution by terrigenous material. The post-event pollen zone (Pz4) is characterised by a decrease in continental and an increase in coastal taxa. Taken together the pollen assemblages comprising the event (Pz2 and Pz3) are clearly of a different source to that pre- (Pz1) and post-event (Pz4), as supported by the DCA.

4.4. Dinoflagellate cyst signatures

Identified dinocyst species are consistent with those reported previously from the Arabian Sea, *e.g.* Zonneveld (1997a, 1997b), Zonneveld and Jurkschat (1999) and are the first reported occurrences along the Makran coastline. The dinocyst zonation (Fig. 3c) shows good agreement with pollen zonations (Fig. 3b) and lithological boundaries (Fig. 3a), identifying the main high-energy event (Fig. 3c). The pre-event dinocyst assemblages contain taxa that typify contemporary upwelling regions and include *Echinidinium* sp. and *B. spongium* as well as neritic species such as *S. quanta* (Fig. 3c). During the event, Dz2 and Dz3 contain high values of *Brigantedinium* sp. and *S. ramosus* which are commonly found in nutrient rich environments such as those with high fluvial discharge (*e.g.* Wall et al., 1977; de Vernal and Giroux, 1989; Marret, 1994). *L. machaerophorum* a species that is known to tolerate a wide range of salinities (*e.g.* Lewis and Hallett, 1997) decreases during Dz2 and Dz3 (Fig. 3c). The post-event assemblage (Dz4) consists of the reoccurrence of upwelling taxa such as *Echinidinium* sp. and *B. spongium. S. quanta* is also observed to increase towards pre-event percentages. Dz4 is characterised by a decrease in the percentage of *Brigantedinium* sp. signifying a decrease in productivity to background levels (Fig. 3c).

4.5. Depositional mechanism: tsunami, cyclone or coastal flood?

The coarse grained, high-energy event unit at 64.5–43 cm shows a basal erosional contact and contains poorly sorted material (Section 3.2), features characteristic of a high energy deposit possibly caused by a tsunami, storm or coastal flood. Sedimentological criteria are not diagnostic in the core examined here, emphasising the need for multi-proxy study to discriminate the depositional mechanism.

Sedimentological and palynological data from core OS55 provide evidence that the largest event within core OS55 occurred between 64.5 and 43 cm (Fig. 3). Poor preservation and low concentrations of both pollen and dinocyst imply that the sediment comprising the high-energy event was most probably deposited quickly. Crucially, the pollen taxa indicate that the sediment comprising the high-energy event unit is not sourced from the coastline. Increases in continental and river taxa (*Betula*, *Typha-Sparganium* and *Salix*) provide direct evidence that the high-energy event unit was due to a flood. It may be argued that a tsunami backwash is the depositional mechanism; however, if the deposit was of tsunami origin, it is probable that coastal sediment would also be incorporated into the event bed (containing an increase in *Rhizophora*), which is not observed. We envisage that an episodic flood, along a river flowing from either Pozm, or Chabahar Bay brought continental sediment into the coring vicinity. Dinocyst taxa provide supportive evidence for the flood hypothesis, with an assemblage characteristic of enhanced productivity (implied by an increase in *Brigantedinium* sp. and *S. ramosus*). Transportation of dinocysts from an area of high productivity (*i.e.* brackish waters), may be responsible for this change in assemblage.

Given our chronology, and the associated uncertainties, we initially identified two potential causative mechanisms to explain the observed event horizon between 64.5 and 43 cm (Section 4.1). We argue that the continentally derived pollen taxa are unequivocal evidence that the event horizon represents a flood deposit. Historically the closest recorded storm and flood event to <AD 1808 is the Arabian Sea storm of AD 1842. Without instrumental measurement, trajectories and intensities of this storm are unknown (Knapp et al., 2010). Our chronology is unable to resolve these two events. Consequently, we suggest the event dated at <AD 1808 (±41), is the geological expression of a flash flood caused by the storm of AD 1842.

Recent large events such as Cyclone Gonu (2007) and the Makran tsunami (1945) are not identified from our GS and palynological records (Fig. 3). It has been suggested that such events may manifest as hiatus' within the geological record representing episodes of erosion (Dawson and Shi, 2000). This is not supported by our ^{210}Pb chronology (Fig. 2) which shows no large-scale removal or remobilisation of sediment post ~AD 1808. Taken together these observations suggest the event at <AD 1808 ± 41 had greater impact, caused by either a more localised source of sediment disturbance, or that the magnitude of the <AD 1808 ± 41 event greatly exceeded those listed historically. Considering evidence from the pollen and dinoflagellate analysis, we favour a more localised mechanism and suggest that the event is the product of a flood from the continental interior (Fig. 3b; c).

5. Conclusion

A multi-proxy analysis of sediment core OS55 from the northern Arabian Sea was used to distinguish the stratigraphic signature of tsunami, storm and flood events around Chabahar Bay, southern Iran. MS and geochemical methods (% $CaCO_3$, % TOC, % TN and % TS) failed to identify the existence of any abrupt event within core OS55. GS determination identified the presence of smaller event beds at 90–88, 77–75, 28.5–27.5, 26–25, 19–17, 12–10 and 9–7 cm (Section 3.2) and a large event bed at 64.5–43 cm, but proved to be non-diagnostic in identifying the mode of emplacement. In contrast palynological approaches (pollen and dinocyst analysis) allowed us to both identify and provenance the event horizon at 64.5–43 cm. The distinct changes in pollen and dinocyst assemblages allow the provenance of the sediment to be inferred and implicate a continentally sourced flash flood as the depositional mechanism.

Although previous studies have suggested 'heading offshore' to search for the sedimentary signature of tsunami and storm deposits (Dawson and Stewart, 2007), we have been unable to find evidence for many of the historically recorded tsunami and storms from the Iranian coast. This study highlights the problem of the preservation of event deposits within the geological record (Einsele et al., 1996; Clifton, 1988; Dawson and Stewart, 2007; Horton et al., 2011; Szczuciński, 2011; Goff et al., 2012; Yawsangratt et al., 2012). Nevertheless, this investigation provides geological evidence on the southern Iranian coast for the storm of AD 1842 and that palynology can be used successfully to identify the existence and cause of abrupt events when other traditional methods may fail. Further investigation into tsunami and storm deposits on the coastline may aid in expanding the palaeoevent database and increase understanding of the frequency and intensity of these

events, which may pose threat to the expanding populations along the coastlines of the northwest Indian Ocean.

Acknowledgements

CSM would like to thank L. Miller, G. Miller and Brunel University for financial support. Gratitude is extended to S. Kershaw and C. Baeteman for useful and pertinent suggestions provided as part of CSM's viva examination. Finally we are grateful to R. Fensome and H. Brinkhuis for discussion regarding species identification.

References

Al-Qurashi, A.M., 2010. Flood studies in Oman and the difficulties in using rainfall run-off analysis. In: Charabi, Y., Al-Hatrushi (Eds.), Indian Ocean Tropical Cyclones and Climate Change. S. Springer-Verlag, New York.
Ambraseys, N.N., Melville, C.P., 1982. A History of Persian Earthquakes. Cambridge University Press, Cambridge.
Appleby, P.G., Oldfield, F., 1978. The calculation of lead-210 dates assuming a constant rate of supply of unsupported ^{210}Pb to the sediment. Catena 5, 1–8.
Appleby, P.G., Birks, H.H., Flower, R.J., 2001. Radiometrically determined dates and sedimentation rates for recent sediments in nine North African wetland lakes (the CASSARINA Project). Aquatic Ecology 35, 347–367.
Bailey, R.W., 1988. Records of Oman: 1867–1947. Archive Editions, Buckingham.
Bennett, K.D., 2003. Documentation for Psimpoll 4.10 and pscomb 1.03: C programs for plotting pollen diagrams and analysing pollen data. Quaternary Geology, University of Uppsala.
Blott, S.J., Pye, K., 2001. GRADISTAT: a grain size distribution and statistics package for the analysis of unconsolidated sediments. Earth Surface Processes and Landforms 26, 1237–1248.
Byrne, D.E., Sykes, L.R., Davis, D.M., 1992. Great thrust earthquakes and aseismic slip along the plate boundary of the Makran subduction zone. Journal of Geophysical Research 97, 449–478.
Chagué-Goff, C., Dawson, S., Goff, J., Zachariasen, J., Berryman, K., Garnett, D., Waldron, H., Mildenhall, D., 2002. A tsunami (ca. 6300 years BP) and other Holocene environmental changes, northern Hawke's Bay, New Zealand. Sedimentary Geology 150, 89–102.
Chagué-Goff, C., Schneider, J.-L., Goff, J., Dominey-Howes, D., Strotz, L., 2011. Expanding the proxy toolkit to help identify past events — lessons from the 2004 Indian Ocean Tsunami and the 2009 South Pacific Tsunami. Earth-Science Reviews 107, 107–122.
Chagué-Goff, C., Goff, J., Nichol, S.L., Dudley, W., Zewadzki, A., Bennett, J.W., Mooney, S.D., Fierro, D., Heijnis, H., Dominey-Howes, D., Courtney, C., 2012. Multi-proxy evidence for trans-Pacific tsunamis in the Hawai'ian Islands. Marine Geology 299–302, 77–89.
Clifton, H.E., 1988. Sedimentological consequences of convulsive geologic events. Geological Society of America 229, 7–22.
Costa, P.J.M., Leroy, S.A.G., Dinis, J.L., Dawson, A.G., Kortekaas, S., 2012. Recent high-energy marine events in the sediments of Lagoa de Obidos and Martinhal (Portugal): recognition, age and likely causes. Natural Hazards and Earth System Sciences 12, 1367–1380.
Dawson, A.G., Shi, S., 2000. Tsunami deposits. Pure and Applied Geophysics 157, 875–897.
Dawson, A.G., Stewart, I., 2007. Tsunami deposits in the geological record. Sedimentary Geology 200, 166–183.
De Vernal, A., Giroux, L., 1989. Distribution of organic walled microfossils in recent sediments from the estuary and Gulf of St. Lawrence. Canadian Special Publication of Fisheries and Aquatic Sciences 113, 198–199.
Dominey-Howes, D.T.M., Humphreys, G.S., Hesse, P.P., 2006. Tsunami and palaeotsunami depositional signatures and their potential value in understanding the late-Holocene tsunami record. The Holocene 16, 1095–1107.
Einsele, G., Chough, S.K., Shiki, T., 1996. Depositional events and their records — an introduction. Sedimentary Geology 104, 1–9.
Faegri, K., Iversen, J., 1989. Textbook of Pollen Analysis. Wiley, Chichester.
Folk, R.L., Ward, W., 1957. Brazos River bar: a study in the significance of grain size parameter. Journal of Sedimentary Petrology 41, 3–26.
Friedman, G.M., 1962. On sorting, sorting coefficients and the log normality of the grain-size distributions of sandstones. Journal of Geology 70, 737–753.
Fritz, H.M., Blount, C.D., Albusaidi, F.B., Al-Harthy, A.H.M., 2010. Cyclone Gonu storm surge in Oman. Estuarine, Coastal and Shelf Science 86, 102–106.
Goff, J., McFadgen, B., Chagué-Goff, C., 2004. Sedimentary differences between the 2002 Easter storm and the 15th-century Okoropunga tsunami, southeastern North Island, New Zealand. Marine Geology 204, 235–260.
Goff, J., Nichol, S., Kennedy, D., 2010. Development of a tsunami database for New Zealand. Natural Hazards 54, 193–208.
Goff, J., Chagué-Goff, C., Nichol, S., Jaffe, B., Dominey-Howes, D., 2012. Progress in palaeotsunami research. Sedimentary Geology 243–244, 70–88.
Harinarayana, T., Hirata, N., 2005. Destructive earthquake and disastrous tsunami in the Indian Ocean, what next? Gondwana Research (Gondwana Newsletter Section) 8, 246–257.
Heidarzadeh, M., Pirooz, M.D., Zaker, N.H., Yalciner, A.C., Mokhtari, M., Esmaeily, A., 2008. Historical tsunami in the Makran Subduction Zone off the southern coasts of Iran and Pakistan and results of numerical modeling. Ocean Engineering 35, 774–786.
Horton, B.P., Sawai, Y., Hawkes, A.D., Witter, R.C., 2011. Sedimentology and paleontology of a tsunami deposit accompanying the great Chilean earthquake of February 2010. Marine Micropaleontology 79, 132–138.
Knapp, K.R., Kruk, M.C., Levinson, D.H., Diamond, H.J., Neumann, C.J., 2010. The International Best Track Archive for Climate Stewardship (IBTrACS): unifying tropical cyclone best track data. Bulletin of the American Meteorological Society 91, 363–376.
Kortekaas, S., Dawson, A.G., 2007. Distinguishing tsunami and storm deposits: an example from Martinhal, SW Portugal. Sedimentary Geology 200, 208–221.
Leroy, S.A.G., Boyraz, S., Gürbüz, A., 2009. High-resolution palynological analysis in Lake Sapanca as a tool to detect earthquakes on the North Anatolian Fault. Quaternary Science Reviews 28, 2616–2632.
Lewis, J., Hallett, R., 1997. *Lingulodinium polyedrum* (*Gonyaulax polyedra*) a blooming dinoflagellate. Oceanography and Marine Biology: An Annual Review 35, 97–161.
Marret, F., 1993. Les effets de l'acétolyse sur les assemblages de kystes de dinoflagellés. Palynosciences 2, 267–272.
Marret, F., 1994. Distribution of dinoflagellate cysts in recent marine sediments from the east Equatorial Atlantic (Gulf of Guinea). Review of Palaeobotany and Palynology 84, 1–22.
McLaren, P.A., 1981. An interpretation of trends in grain size measures. Journal of Sedimentary Research 51, 611–624.
McLaren, P.A., Bowles, D., 1985. The effects of sediment transport on grain-size distribution. Journal of Sedimentary Petrology 55, 457–470.
Morton, R.A., Gelfenbaum, G., Jaffe, B.E., 2007. Physical criteria for distinguishing sandy tsunami and storm deposits using modern examples. Sedimentary Geology 200, 184–207.
Quittmeyer, R.C., Jacob, K.H., 1979. Historical and modern seismicity of Pakistan, Afghanistan, northwestern India, and southeastern Iran. Bulletin of the Seismological Society of America 69, 773–823.
Ramanathan, A.L., Rajkumar, K., Majumdar, J., Singh, G., Behera, P.N., Santra, S.C., Chidambaram, D., 2009. Textural characteristics of the surface sediments of a tropical mangrove Sundarban ecosystem India. Indian Journal of Marine Sciences 38, 397–403.
Ramírez-Herrera, M.-T., Lagos, M., Hutchinson, I., Kostoglodov, V., Machain, M.L., Caballero, M., Goguitchaichvili, A., Aguilar, B., Chagué-Goff, C., Goff, J., Ruiz-Fernández, A.-C., Ortiz, M., Nava, H., Bautista, F., Lopez, G.I., Quintana, P., 2012. Extreme wave deposits on the Pacific coast of Mexico: tsunamis or storms? — A multi-proxy approach. Geomorphology 139–140, 360–371.
Reille, M., 1995. Pollen et Spores D'Europe et D'Afrique du Nord. Laboratoire de Botanique historique et Palynologie, Marseille.
Ritchie, J.C., McHenry, J.R., 1990. Application of radioactive fallout cesium-137 for measuring soil erosion and sediment accumulation rates and patterns: a review. Journal of Environmental Quality 19, 215–233.
Rochon, A., Vernal, A., de Turon, J.-L., Matthiessen, J., Head, M.J., 1999. Distribution of recent dinoflagellate cysts in surface sediments from the North Atlantic Ocean and adjacent seas in relation to sea-surface parameters. American Association of Stratigraphic Palynologists Contributions Series 35, Dallas, TX.
Saket, A., Etemad-Shahidi, A., 2012. Wave energy potential along the northern coasts of the Gulf of Oman, Iran. Renewable Energy 40, 90–97.
Shah-hosseini, M., Morhange, C., Naderi Beni, A., Marriner, Lahijani, H., Hamzeh, M., Sabatier, F., 2011. Coastal boulders as evidence for high-energy waves on the Iranian coast of Makran. Marine Geology 290, 17–28.
Stockmarr, J., 1972. Tablets with spores used in absolute pollen analysis. Pollen et Spores XIII, 615–621.
Szczuciński, W., 2011. The post-depositional changes of the onshore 2004 tsunami deposits on the Andaman Sea coast of Thailand. Natural Hazards 60, 115–133.
Tucker, M.E., 1981. Sedimentary petrology: an introduction. Geoscience Texts, volume 3. Blackwell Scientific.
Twiddle, C.L., Bunting, M.J., 2010. Experimental investigations into the preservation of pollen grains. Review of Palaeobotany and Palynology 162, 621–630.
Wall, D., Dale, B., Lohmann, G.P., Smith, W.K., 1977. The environmental and climatic distribution of dinoflagellate cysts in modern marine sediments from regions in the North and South Atlantic Oceans and adjacent seas. Marine Micropaleontology 2 (77), 121–200.
Webster, P.J., Holland, G.J., Curry, J.A., Chang, H.-R., 2005. Changes in tropical cyclone number, duration, and intensity in a warming environment. Science 309, 1844–1846.
Yawsangratt, S., Szczuchński, W., Chaimanee, N., Chatprasert, S., Majewski, W., Lorenc, S., 2012. Evidence of probable paleotsunami deposits on Kho Khao Island, Phang Nga Province, Thailand. Natural Hazards 63, 151–163.
Zohary, M., 1973. Geobotanical foundations of the Middle East, vol 1. Gustav Fischer Verlag, Berlin.
Zonneveld, K.A.F., 1997a. Dinoflagellate cyst distribution in surface sediments from the Arabian Sea (northwestern Indian Ocean) in relation to temperature and salinity gradients in the upper water column. Deep Sea Research Part II: Topical Studies in Oceanography 44, 1411–1443.
Zonneveld, K.A.F., 1997b. New species of organic walled dinoflagellate cysts from modern sediments of the Arabian Sea (Indian Ocean). Review of Palaeobotany and Palynology 97, 319–337.
Zonneveld, K.A.F., Jurkschat, T., 1999. *Bitectatodinium spongium* (Zonneveld, 1997) Zonneveld et Jurkschat, comb. nov. from modern sediments and sediment trap samples of the Arabian Sea (northwestern Indian Ocean): taxonomy and ecological affinity. Review of Palaeobotany and Palynology 106, 153–169.